Journal of Power Sources 274 (2015) 1208–1216

Contents lists available at ScienceDirect

Journal of Power Sources

journal homepage: www.elsevier.com/locate/jpowsour

Mechanical degradation of fuel cell membranes under fatigue fracture tests

Ramin M.H. Khorasany, Alireza Sadeghi Alavijeh, Erik Kjeang*, G.G. Wang, R.K.N.D. Rajapakse

School of Mechatronic Systems Engineering, Simon Fraser University, 250-13450 102 Avenue, Surrey, BC, V3T 0A3, Canada

HIGHLIGHTS

- An ex-situ tensile fatigue fracture test of fuel cell membranes is proposed.
- The membrane fatigue lifetime is a function of stress, temperature, and humidity.
- The effect of temperature on fatigue life is stronger than that of humidity.
- A critical level of elongation is shown to lead to membrane fracture.

GRAPHICAL ABSTRACT

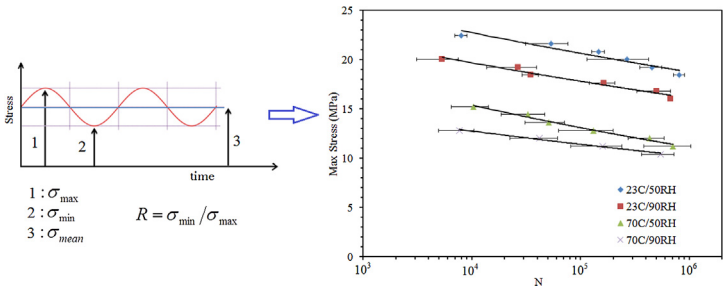

ARTICLE INFO

Article history:
Received 15 July 2014
Received in revised form
14 October 2014
Accepted 21 October 2014
Available online 28 October 2014

Keywords:
Fuel cell
Membrane
Fatigue
Fracture
Degradation
Durability

ABSTRACT

The effects of cyclic stresses on the fatigue and mechanical stability of perfluorosulfonic acid (PFSA) membranes are experimentally investigated under standard fuel cell conditions. The experiments are conducted ex-situ by subjecting membrane specimens to cyclic uniaxial tension at controlled temperature and relative humidity. The fatigue lifetime is measured in terms of the number of cycles until ultimate fracture. The results indicate that the membrane fatigue lifetime is a strong function of the applied stress, temperature, and relative humidity. The fatigue life increases exponentially with reduced stresses in all cases. The effect of temperature is found to be more significant than that of humidity, with reduced fatigue life at high temperatures. The maximum membrane strain at fracture is determined to decrease exponentially with increasing membrane lifetime. At a given fatigue life, a membrane exposed to fuel cell conditions is shown to accommodate more plastic strain before fracture than one exposed to room conditions. Overall, the proposed ex-situ membrane fatigue experiment can be utilized to benchmark the fatigue lifetime of new materials in a fraction of the time and cost associated with conventional in-situ accelerated stress testing methods.

1. Introduction

The polymer electrolyte fuel cell (PEFC) is a promising clean energy technology for converting chemical energy into electrical energy. PEFCs have a wide range of applications including uses in cars, heavy-duty vehicles, materials handling, and backup power systems. Widespread uses of this technology can be of a great benefit to the environment through reducing greenhouse gas emissions [1]. A typical PEFC consists of a membrane electrode assembly (MEA) situated between two flow field plates. The MEA is composed of an ion-conducting membrane flanked by two electrodes (anode and cathode) and two gas diffusion layers.

* Corresponding author.
E-mail address: ekjeang@sfu.ca (E. Kjeang).

http://dx.doi.org/10.1016/j.jpowsour.2014.10.135
0378-7753/

Generating clean energy from hydrogen fuel cells has been the subject of numerous scholarly works ranging from low-power micro fuel cells [2] to high-power fuel cell stacks [3–5].

One of the major technical challenges of polymer electrode fuel cells is the durability of the MEA under dynamic operating conditions [1]. The stability of the MEA is commonly limited by the initiation of pinholes and micro cracks in the membrane, which may lead to undesirable hydrogen leaks, performance losses, and ultimate failure. Membrane damage can be initiated and propagated as a result of chemical and mechanical degradation mechanisms. Chemical degradation has been widely studied in the literature [5]. It has been reported that factors such as contamination of transition metal ion, reactant gas crossover, and variation in the temperature and potential have direct effect on the chemical degradation of commonly used perfluorosulfonic acid (PFSA) ionomer membranes [6,7]. Open circuit voltage (OCV) operation has been established as an in-situ accelerated stress test to accelerate the rate of chemical degradation [8,9]. A significant body of work is available on chemical membrane degradation mechanisms and mitigation strategies [10–18].

It is well known that the mechanical response of the membrane to dynamic operating conditions depends on the loading rate [19–21]. Furthermore, when the membrane is subjected to a constant strain, the stress relaxes over time [20]. On the other hand, the membrane also exhibits mechanical creep due to sliding of the polymer chains with respect to one another when subjected to a constant stress [21]. Ex-situ mechanical testing of the membrane has been widely used to determine its properties and ability to respond to applied stress [19,22]. The mechanical properties were found to vary with environmental conditions [23,24]. At elevated levels of environmental conditions, the elastic modulus and yield point of the membrane substantially decreased [22,25]. The creep and relaxation behavior of the membrane is also affected by the environmental conditions. At elevated levels of relative humidity, the stress relaxation time was shown to decrease due to the lower driving force [26]. Furthermore, the creep strain of the membrane increased with elevated temperature [27]. A previous experimental study by our group [19] revealed that catalyst coated membranes exhibit significantly different mechanical behavior than pure PFSA membranes, and would therefore respond differently under externally applied loads.

While chemical membrane degradation is one of the main stressors in membrane thinning and ultimate failure of the MEA, mechanical degradation is also considered to play a significant role in initiation and propagation of micro cracks and fractures inside the membrane. The membrane water absorption-desorption that occurs during typical fuel cell duty cycles causes swelling and contraction in the membrane [28]. As a result, dynamic stress patterns are created in the membrane that ultimately limit the membrane life due to fatigue and fracture. Ex-situ mechanical degradation has been studied by exposing the membrane to cyclic environmental conditions [29] or uniaxial mechanical loading [30]. In-situ mechanical accelerated stress testing was generally performed using wet/dry humidity cycles [9,31–34]. Lim et al. [35] applied an advanced accelerated stress test protocol to simultaneously study the effect of chemical and mechanical degradation mechanisms on the properties of the membrane.

Modeling the ex-situ and in-situ response of the membrane under hygrothermal and mechanical loadings is another challenge in further understanding the mechanical degradation process of the membrane [22,36,37]. In earlier attempts [34], linear elastic and plastic behavior with isotropic hardening was adopted for the response of the membrane. As stated earlier, due to time dependency of the response, such models cannot fully represent the mechanical behavior of the membrane [19]. It was shown that adopting an elastic-viscoplastic model cannot only capture the time-dependent response of the membrane but is also capable of predicting the response in different hygrothermal conditions [38]. These models were then used to study the effect of ex-situ biaxial tensioning on the membrane [39].

In previously published results, the mechanical stability of the membrane was found to be significantly affected by the cyclic change in the environmental conditions and in particular by cyclic changes in the relative humidity (RH) [29]. However, the membrane yield stress and yield strain did not change due to RH cycling. Conversely, with deep RH cycles, the strain to failure was found to significantly drop [29]. Two different approaches have been established regarding the failure determination of the membrane under mechanical cyclic loadings. In the first approach, the surface cracks on the membrane are monitored until a critical crack density is reached [40,41]. In the second approach, the failure of the membrane is defined as the mechanical rupture of the specimen [21,30,42,43]. Compared to the second approach [30], the first approach [29] predicts a significantly lower number of cycles to failure.

While mechanical degradation has been studied extensively using both ex-situ and in-situ techniques [16,44], as described above, the process of material *fatigue* leading to micro crack initiation and ultimate fracture propagation and failure is not yet well understood. For other more common materials such as metals, fatigue is a well-established concept and its role in material degradation and failure has been proven through comprehensive research and testing [45,46]. Hence, the main objective of the present work is to develop a comprehensive, fundamental understanding of the fatigue-fracture behavior of typical ionomer membranes during conditions relevant for fuel cell operation. An ex-situ tensile fatigue experiment is designed to characterize the effect of mechanically induced cyclic loadings on the fatigue lifetime of the membrane under a range of environmental conditions. A statistical design of experiments approach is employed to investigate the effects of relative humidity and temperature on the maximum stress and strain before the rupture. The proposed fatigue-fracture experiment is intended to shed light on the complex mechanical membrane degradation mechanism and can potentially be utilized as an ex-situ alternative to conventional in-situ accelerated stress tests for mechanical membrane durability.

2. Experimental technique

2.1. Materials

Commercially available Nafion® NR-211 perfluorosulfonic acid (PFSA) ionomer membrane specimens of 25 μm thickness were prepared from a single batch of material to warrant the consistency of the results. To reduce the effect of stress concentration in the clamping area, the specimens were cut in dog bone shapes, using the die shape illustrated in Fig. 1. The same geometry was previously used for a different type of membrane [30]; however, the

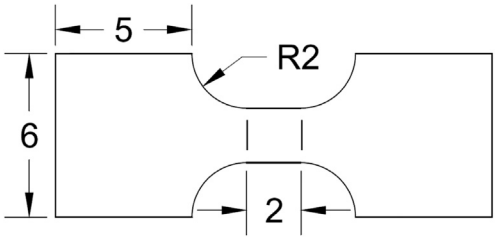

Fig. 1. Schematic of the specimen geometry with two marks to identify its straight portion (mm).

dimensions were slightly modified to account for the higher ductility of the present membrane material. During the cutting process the membrane sheet was placed on a hardened plate made of tool steel, with the membrane backing sheet facing the plate. The membrane was covered by a thin sheet of paper to avoid inaccuracies during cutting. Using a hydraulic press, the die was pressed against the prepared sandwich. The specimens were cut in the cross-machine (transverse) direction. The quality of the obtained specimens was visually confirmed with an optical microscope before testing. Lastly, the specimen width and thickness were measured using the optical microscope and a digital micrometer, respectively.

2.2. Test apparatus and procedure

The fatigue experiments were performed using a Dynamic Mechanical Analyzer (TA Instruments Q800 DMA) with humidity accessory. For each test, a specimen was loaded at room conditions in the DMA chamber with a small preload force (0.001–0.005 N). The specimens were installed with the DMA grips covering the entire rectangular end sections without overlapping the curved central section intended for fatigue characterization (*cf.*, Fig. 1). The temperature and humidity levels were brought to desired conditions and allowed enough time to equilibrate. Once the rate of lengthwise swelling and thermal expansion was measured to be less than 1 μm min^{-1}, the test was started. In each fatigue test a predefined constant mean force and a superimposed cyclic sinusoidal mechanical force were applied. The frequency of the cyclic load was 10 Hz, and the maximum stress was chosen based on a minimum to maximum stress ratio (R) of 0.2. To study how the dynamic force amplitude changes the fatigue properties of the membrane, two additional R values, 0.4 and 0.6, were considered and tested in the room condition by adjusting the mean stress.

The failure criterion applied in this work was defined as the final mechanical rupture of the specimen, which assumes that the time to crack initiation by fatigue dominates the time for crack propagation and fracture formation in the membrane. Previously published works suggest that PFSA membranes experience significant plastic strain before reaching mechanical failure [19,21]. Indeed, our previous in-situ finite element simulations indicated that the stresses generated during typical hygrothermal cycles cause significant plastic strain inside the membrane [28].

A 2^2 factorial experiment was designed to evaluate the effects of relative humidity and temperature on the maximum stress level and strain to failure of the specimen. The two factors, relative humidity and temperature, were varied jointly across a range of relevant fuel cell conditions. The two extreme cases in this study were the room condition with 23 °C, 50% RH and the fuel cell condition with 70 °C, 90% RH. Two more corner points were also taken into account to complete the matrix: 23 °C, 90% RH and 70 °C, 50% RH. At least three specimens were tested at each condition. A standard F test based analysis of variance (ANOVA) was performed to determine the statistical effects of temperature and humidity and their interaction by comparing the means at each environmental condition. The F test is a widely used method for the determination of the statistical significance of various factors and their interactions on a response variable. In the present case, a p value of 0.05 was used as a threshold, which corresponds to a confidence level of 95%. The statistical assessment of the interaction effects was supported by interaction plots to illustrate the coupling of the factors.

2.3. Stress selection

Selection of an appropriate stress level is an important consideration for fatigue fracture experiments to ensure the validity of the results. Previously measured tensile stress–strain curves by our group [19] were utilized for this purpose. The relevant data in Fig. 2 shows true stress plotted against true strain at four different combinations of temperature and relative humidity. The mean value of the cyclic fatigue stress was chosen to facilitate a maximum stress above the yield stress in each condition. The strain rate that was used for obtaining the stress–strain curves plotted in Fig. 2 was 0.01 min^{-1}. Previous studies [19,38] have indicated that due to viscoplastic characteristics of the membrane, increasing the strain rate by an order of magnitude may raise the yield stress by around 10–15%. The effect of strain rate was therefore accounted for in the stress selection for the fatigue experiments.

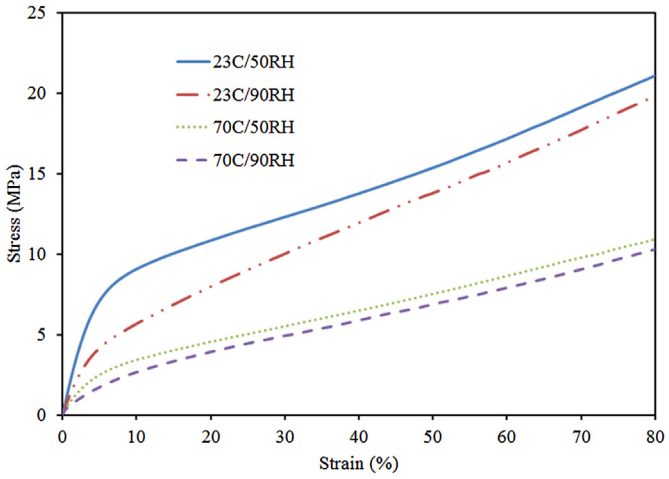

Fig. 2. Tensile stress–strain curves at four different environmental conditions.

The stress applied in fatigue experiments is composed of a mean stress value coupled with an oscillating stress, as illustrated in Fig. 3. The amplitude of the stress oscillations depends upon the mean value of the stress to ensure that the chosen R value (minimum to maximum stress ratio) for the experiments is reached. Studies for other materials have indicated that both the mean stress and the amplitude of the stress oscillations play a role in the fatigue process. However, the effect of the stress amplitude is the dominant factor [45,46]. Membranes situated inside fuel cells are constrained by adjacent components and experience both positive (tensile) and negative (compressive) stresses induced by swelling and contraction due to hygrothermal variations during fuel cell operation [47]. In terms of fatigue, the effect of stress amplitude is therefore expected to be more significant that the effect of mean stress. The function of the applied mean stress in the ex-situ tests is similar to the action of confinement for in-situ applications. The proposed tensile fatigue test can however only apply positive stress. Hence, in order to generate a stress amplitude that resembles the in-situ

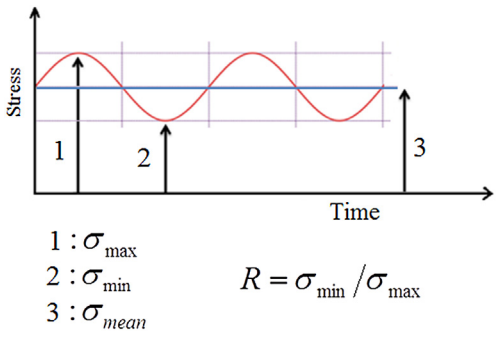

Fig. 3. Schematic of the stress profile versus time.

conditions as much as possible, a small R value of 0.2 was chosen, which minimizes the maximum stress while retaining the appropriate stress amplitude.

The membrane has a time dependent behavior, meaning that the stress response is rate dependent and the stress relaxes over time [48]. During fuel cell operating cycles from room conditions (23 °C, 50% RH) to fuel cell conditions (70 °C, 90% RH) the amplitude of the relaxed stress oscillations (true stress) was simulated to be 6.0 MPa [28]. However, with more severe hygrothermal cyclic loading conditions the amplitude of relaxed stress oscillations can be even higher than 11 MPa [47]. In cases where the time dependency characteristic of the membrane is taken into account, a peak stress before the relaxation is experienced by the membrane, which is significantly higher than the relaxed stress level. According to simulations conducted by Silberstein et al. [47] the amplitude of the peak stress can be up to 30% higher than the relaxed stress. The amount of stress relaxation also depends upon the loading conditions [47,49]. For a pure RH cycle, Khattra et al. [49] predicted that the peak stress can be up to 100% higher than the relaxed stress. Furthermore, the width and orientation of the land and channel sections can also change the stress profile inside the membrane. In the study conducted by Lu et al. [50] using wide, alternating channels, the relaxed stress at the dried state reached 17 MPa. This also indicates that for the alternating configuration, the peak stress before relaxation can be well above 20 MPa, according to Khattra et al. [49]. Thus, depending on the loading conditions and cell geometry, the stress amplitude (true stress) can range from 8 to 25 MPa. In the present fatigue experiments, a wide range of stress amplitudes that correspond to fuel cell conditions as discussed above were tested.

2.4. Determination of plastic strain

One interesting aspect of the fatigue experiments is the maximum deformation incurred before the mechanical failure. The total specimen elongation was therefore tracked during the experiments. However, due to the dog bone specimen shape the local strains in the curved and straight portions differ significantly and the ultimate plastic deformation cannot be calculated directly. Therefore, to find the amount of plastic strain in the central, straight portion before the final fatigue fracture, a separate series of experiments were conducted. In these experiments, the specimens were marked to identify the straight portion (Fig. 1) such that its length could be tracked during cyclic fatigue loading. The experiments were halted shortly before final fracture with the tensile clamp fixture locked in its final position, which allows the humidity chamber to be evacuated and opened in order to record the total elongation. This procedure was repeated at least four times for each set of environmental conditions. For the strain-time curves, additional tests were conducted to measure the elongation of the central, straight portion of the specimen as a function of the total elongation. A mapping between the length of the straight portion and the total elongation of the specimen was established and used to generate strain-time curves.

The final engineering and true strains of the straight portion were calculated by Ref. [36]:

$$\varepsilon^{\mathrm{eng}} = \frac{\Delta L}{L} \tag{1}$$

$$\varepsilon^{\mathrm{true}} = \ln\left(1 + \varepsilon^{\mathrm{eng}}\right) \tag{2}$$

where L and ΔL are the initial length and total elongation of the straight portion of the specimen. A separate experiment was performed at each set of environmental conditions to determine the initial length after equilibration.

3. Results and discussions

3.1. S–N curves

The fatigue life of the membrane was measured as the number of cycles to mechanical failure (N) for various levels of maximum engineering stress (S). A baseline minimum to maximum stress ratio (R) of 0.2 was applied in all experiments unless otherwise stated. The stress-life (S–N) curves obtained at the four different environmental conditions investigated in this study are illustrated in Fig. 4.

In agreement with the literature [30], the number of cycles until mechanical failure is found to increase exponentially with the decreasing maximum stress under all considered environmental conditions. Interestingly, the S–N curves at 23 °C, 50% RH and 23 °C, 90% RH are almost parallel with a significant vertical shift induced by the lower humidity condition. This shift is related to the significant difference in yield stress at these two conditions, as shown in Fig. 2. The shift between the S–N curves at 70 °C, 50% RH and 70 °C, 90% RH (Fig. 4) is less significant due to the more similar yield stresses at this temperature (Fig. 2). More importantly, the fatigue life is found to decrease substantially with increasing temperature, as the membrane becomes softer and more prone to plastic deformation when heated. Elevation in temperature and relative humidity is known to decrease the ultimate tensile stress of the membrane [19,21], which is in agreement with the present findings for fatigue. Furthermore, as the temperature and relative humidity levels change from room conditions to fuel cell conditions, the slope of the S–N curves is found to decrease. This indicates that the fatigue life is more sensitive to stress at the fuel cell condition than at the room condition. Consequently, a small reduction in maximum stress during fuel cell operation may have a large positive effect on membrane fatigue life. Pestrak et al. [51] conducted blister tests under mechanical cyclic pressure loadings to study the fatigue lifetime of the membrane. Given that the true state of stress is difficult to estimate in blister tests, the effect of the amplitude of cyclic loadings cannot be thoroughly investigated. In contrast, the present tensile fatigue test provides a clear relation between the amplitude and mean value of the stress and the membrane lifetime.

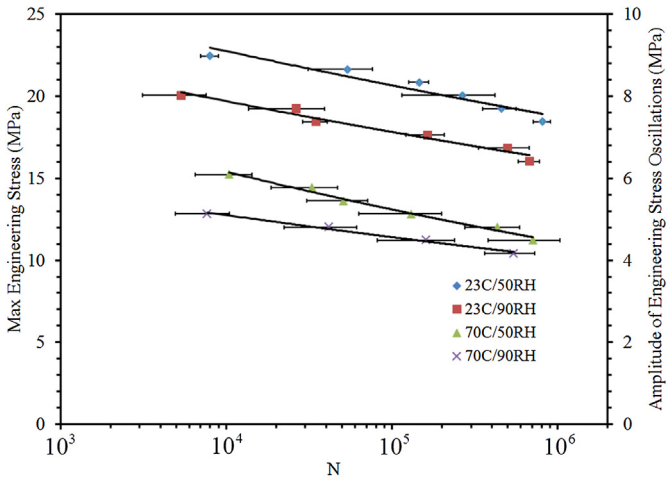

Fig. 4. Measured fatigue life curves in the form of maximum engineering stress (S) and amplitude of engineering stress oscillations versus the number of cycles to failure (N).

Table 1
ANOVA results for the maximum engineering stress at specific fatigue lifetimes.

	Temperature		Relative humidity		Interaction	
	Effect (MPa)	*p* value	Effect (MPa)	*p* value	Effect (MPa)	*p* value
$N_1 = 2 \times 10^5$	−6.99	<0.001	−2.08	<0.001	0.72	<0.001
$N_2 = 4 \times 10^5$	−6.96	<0.001	−1.92	<0.001	0.83	<0.001
$N_3 = 6 \times 10^5$	−6.94	<0.001	−1.83	<0.001	0.88	<0.001
$N_4 = 8 \times 10^5$	−6.92	<0.001	−1.77	<0.001	0.92	<0.001

To discern the effects of humidity and temperature on the stress level at specific fatigue lifetimes (2×10^5, 4×10^5, 6×10^5 and 8×10^5 cycles), an ANOVA analysis was carried out with key results summarized in Table 1. As expected, an increase in temperature and relative humidity has a negative effect on the maximum stress threshold for a given membrane lifetime. This result is statistically significant in all cases considered here and is primarily caused by the softening effects of the relative humidity and temperature on the membrane mechanical properties (Fig. 2). The relative effect of temperature is however more than three times stronger than the effect of humidity in the presently tested range. Moreover, considering that the magnitude of the temperature effect decreases more slowly than the humidity effect with increasing lifetime (−1% and −18% respectively from N_1 to N_4), the effect of temperature is expected to be particularly important even beyond the fatigue lifetime range considered here.

Due to the stiffening effect caused by the interaction of temperature and relative humidity on the membrane modulus [19], the interaction effect on the maximum stress is positive (Table 1). The interaction effect increases further by ~28% with increasing fatigue lifetime from N_1 to N_4. These results are illustrated graphically in the interaction plot in Fig. 5 for N_1 and N_4, where the difference in slopes between the two lines distinguishes the interaction of the two variables. The interaction is larger at N_4 compared to N_1 and indicates that the effect of humidity on maximum stress is less significant at higher temperatures.

3.2. Plastic strain curves

In a fatigue experiment, the specimen elongates due to plastic deformation and creep. Plastic deformation generally occurs in membranes when high stresses beyond the yield point are applied. Creep occurs under stress by progressive sliding of molecular chains within the polymer matrix. Membrane creep is a function of environmental conditions and increase with both temperature and relative humidity [21]. Plastic strain (deformation) is known to be induced in the membrane as a result of hygrothermal variations during fuel cell operation. Depending on the hygrothermal loading rate and amplitude, the plastic strain in the membrane can reach well above 0.1 [28,47]. These plastic strains are tensile and compressive in the through plane and in plane directions, respectively. During the unloading phase a stress profile in the direction opposite to that of the stress during the loading phase is created in the membrane. As a result, a counteracting plastic strain profile is generated and a portion of the plastic strain in the loading phase is recovered. However, when the membrane is subjected to ex-situ cyclic loadings that are exclusively tensile, there is no opportunity for plastic strain recovery. Hence, strain is accumulated in the tensile direction and creates substantial specimen elongation [38].

Illustrated in Fig. 6 are the strain curves obtained for different levels of the maximum stress at room (23 °C, 50% RH) and fuel cell (70 °C, 90% RH) conditions. The plastic strain is consistently shown to increase with applied maximum stress as the material experiences more rapid plastic deformation when subjected to stresses further beyond the yield point. At high stress, the growth of plastic deformation in the material is expected to play a key role in the rupture process. In agreement with previous reports [21], the maximum strain before mechanical rupture of the specimen is higher at the fuel cell condition than at the room condition. The rate of elongation is also more rapid at the fuel cell condition than at the room condition, as can be expected due to the much lower elastic modulus, yield point, and tangent slope for the post yield behavior

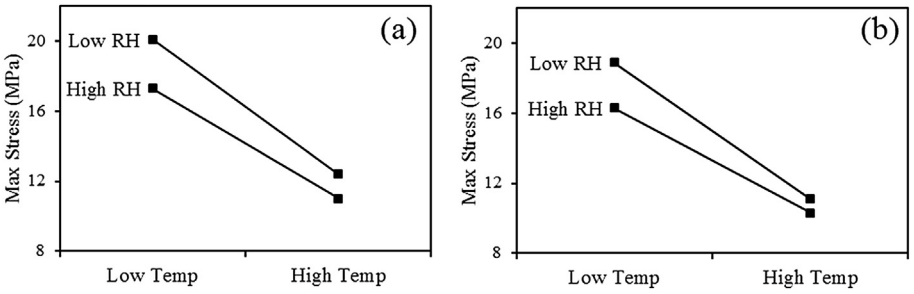

Fig. 5. Interaction plots for the maximum engineering stress at (a) $N_1 = 2 \times 10^5$ and (b) $N_4 = 8 \times 10^5$.

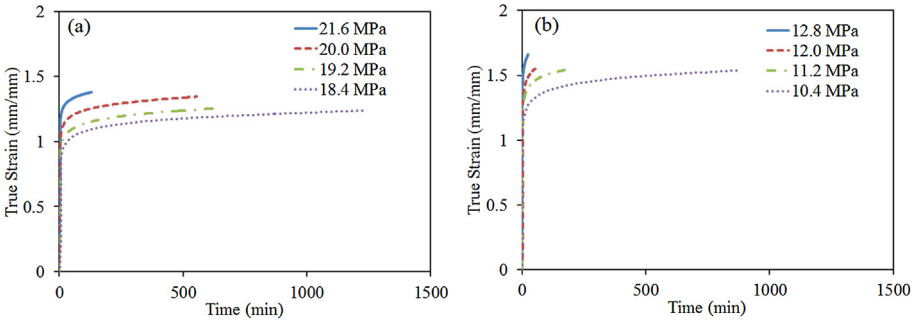

Fig. 6. True strain curves at four different fatigue loading conditions at (a) 23 °C, 50% RH and (b) 70 °C, 90% RH.

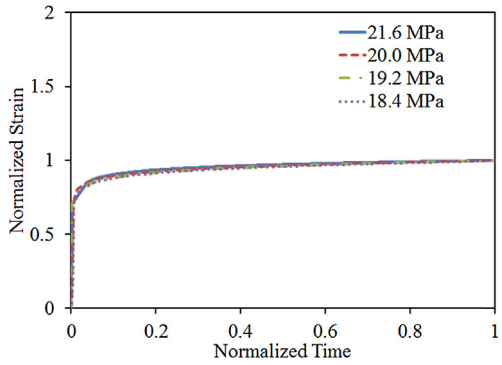

Fig. 7. Normalized strain profile at four different fatigue loading conditions at 23 °C, 50% RH.

(Fig. 2). The results presented in Fig. 6 are in agreement with those reported by Huang et al. [29]. They reported that an MEA subjected to RH cycling can withstand a high amount of plastic strain (e.g., higher than 100% strain) before mechanical rupture. Furthermore, they noted that RH cycling reduced the strain to failure of the specimens. In agreement with their work, it can be deduced from the present fatigue results that the strain to failure is reduced with an increasing number of mechanical fatigue cycles (Fig. 6).

To understand the deformation process of the membrane during the fatigue process under different loading conditions, the strain curves are normalized. The normalized curves at 23 °C, 50% RH, shown in Fig. 7, were obtained by dividing the strain by the maximum strain at rupture and the time by the fatigue lifetime. The normalized strain curves are seen to collapse onto a single curve with less than 1% deviation. This was also observed for the other environmental conditions tested (not shown here). Overall, the normalized strain curves indicate that for all environmental conditions and loading levels considered in this study, the plastic deformation and creep process inside the membrane material is progressing in a common manner.

Another important characteristic of the fatigue failure is to investigate the strain at rupture as a function of the loading condition. Illustrated in Fig. 8 are the strains obtained versus the maximum stress at each environmental condition. Under all environmental conditions, the strain at fracture is seen to grow in a linear pattern with increasing levels of maximum stress, which is believed to be an important fatigue property of ionomer membranes. No major difference in strain is found between room condition and 23 °C, 90% RH, which indicates that the observed range of strain at fracture is essentially independent of relative humidity. However, the strain difference between room condition and the two environmental conditions with higher temperature is significant. It is also observed that the sensitivity of strain to maximum stress is much less significant at the fuel cell condition than for the other three conditions. In terms of mechanical degradation, this finding demonstrates the existence of a critical level of membrane strain (or plastic strain) susceptible to fatigue fracture development under standard fuel cell conditions.

The role of plastic deformation in the fatigue process is further analyzed by investigating the strain at failure as a function of the fatigue lifetime, as shown in Fig. 9. A significant upwards shift in strain is found with increasing temperature. The effect of humidity appears to be more complex. At room conditions, the effect of humidity is minor, whereas at the fuel cell condition, a change in slope is observed with changes in humidity. Perhaps more importantly, the sensitivity of fatigue lifetime to strain at fuel cell condition is found to be high, in agreement with the previous result for the critical level of plastic deformation at fatigue fracture.

An ANOVA analysis is conducted to quantify the effect of temperature and relative humidity on the strain at fracture at fixed levels of fatigue lifetime. The results of the ANOVA analysis are summarized in Table 2. The main effects for both temperature and relative humidity are significant and have positive effect on the fatigue induced strain; however, the main effect of the relative humidity is substantially lower than that of the temperature and only statistically significant at lifetimes above 400,000 cycles. Notably, the effect of temperature is clearly statistically significant

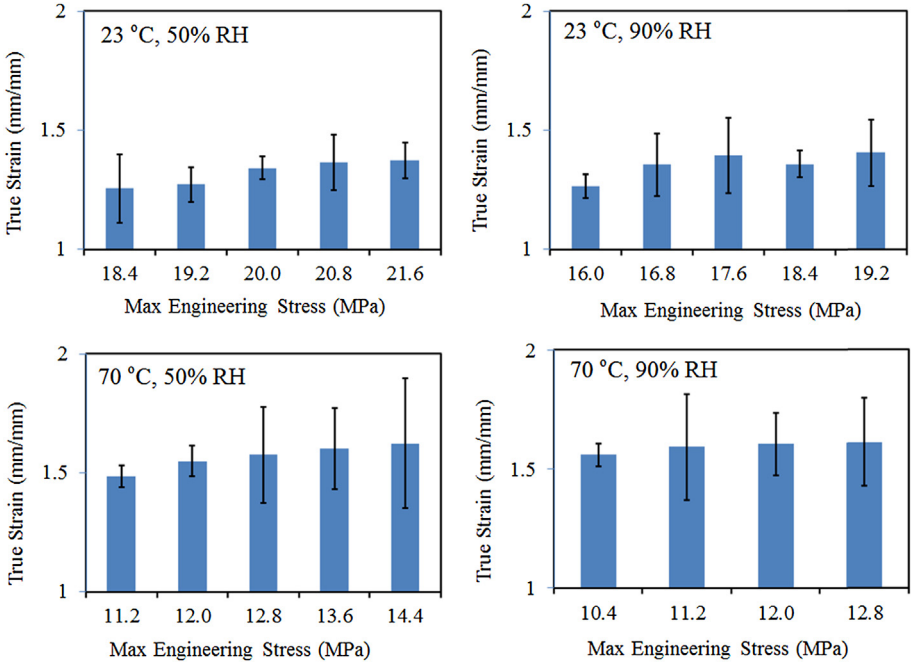

Fig. 8. True strain versus the maximum engineering stress at four different environmental conditions.

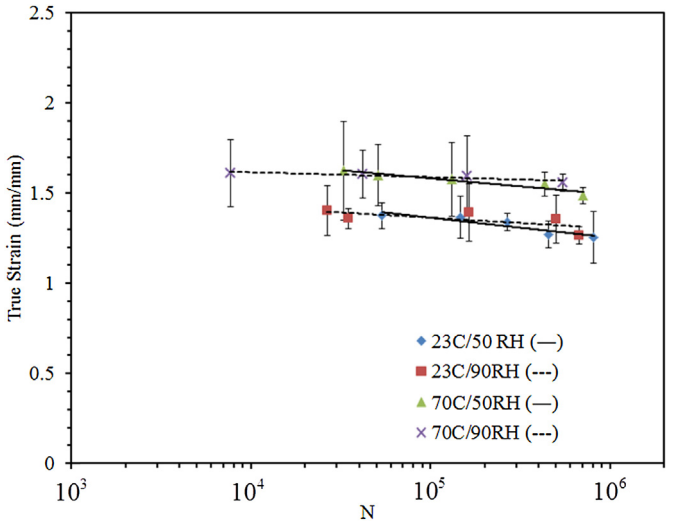

Fig. 9. True strain at fracture versus fatigue lifetime (N) for each environmental condition.

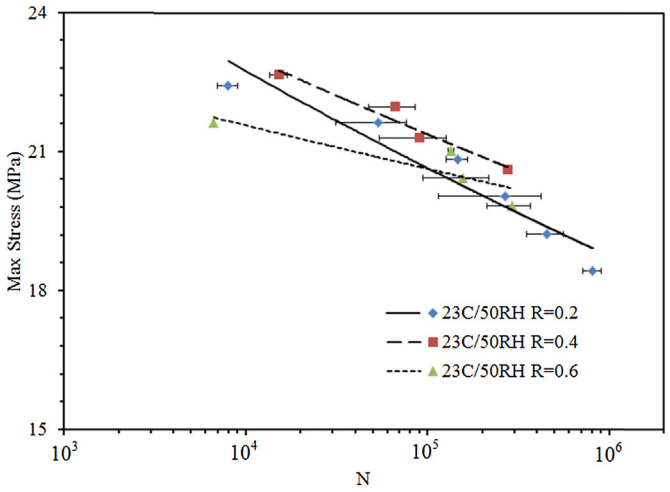

Fig. 11. Fatigue life curves at room conditions for three different stress ratios (R).

Table 2
ANOVA analysis of the strain at specific fatigue lifetimes.

	Temperature		Relative humidity		Interaction	
	Effect (mm/mm)	p value	Effect (mm/mm)	p value	Effect (mm/mm)	p value
$N_1 = 2 \times 10^5$	0.23	<0.001	0.02	0.31	−0.001	0.61
$N_2 = 4 \times 10^5$	0.24	<0.001	0.04	0.002	0.003	0.52
$N_3 = 6 \times 10^5$	0.24	<0.001	0.05	<0.001	0.006	0.22
$N_4 = 8 \times 10^5$	0.25	<0.001	0.06	<0.001	0.008	0.12

with small values of p; while we cannot conclude that for the humidity. The interaction effect is not statistically significant either according to its p values, as confirmed by the parallel lines in the interaction plot provided in Fig. 10.

3.3. The effect of stress ratio

The fatigue lifetime before mechanical failure of the membrane is not only a function of the maximum stress and environmental conditions but also a function of the ratio of the minimum stress to maximum stress (R). For metallic materials, fatigue properties are commonly characterized by using $R = -1$ (alternating compressive and tensile stress) or $R = 0$ (tensile stress with zero minimum stress). However, the thin PFSA membrane specimens cannot absorb compressive loads and using $R = 0$ would create unstable behavior in the DMA during testing. Hence, the feasible range of stress ratio is between 0 and 1. In the present case, $R = 0.2$ was chosen as the baseline stress ratio [30]. Two other R values in the feasible range were also considered for analysis, namely 0.4 and 0.6. Higher R values means a relatively large mean stress, in which case the fatigue will be initially dominated by the creep failure [21].

Illustrated in Fig. 11 are the plots of maximum stress versus fatigue lifetime at $R = 0.2$, 0.4, and 0.6. The tests were conducted at room conditions (23 °C, 50% RH). As expected, once R increases from 0.2 to 0.4, the S–N curve shifts upward, indicating that for a given maximum stress the specimen would last longer at $R = 0.4$ compared to $R = 0.2$. This is a consequence of the smaller amplitude of the cyclic load which reduces the severity of the dynamic fatigue action and leads to longer lifetime.

The case of $R = 0.6$ is somehow different as illustrated in Fig. 11. When the mean stress is substantially large and the amplitude of the fluctuating stress is small, the mechanical failure is predominantly affected by the creep phenomenon [21]. This is demonstrated in our case by the early failures obtained at high maximum stress with $R = 0.6$. As the maximum stress is reduced, the lifetime is rapidly increased into the fatigue dominated regime. The effects of dynamic stress amplitude and mean stress are further investigated in Fig. 12. Most notably, these results demonstrate that the fatigue lifetime test is more sensitive to the mean stress at high R values (e.g., 0.6), as shown by the clustering of the data points, which indicates a strong influence of creep. In contrast, low R values (e.g., 0.2) are less sensitive to mean stress and dominated by fatigue dynamics, which is more desirable in this case.

4. Conclusions

In this article, an ex-situ tensile fatigue experiment was developed to explore the mechanical stability of fuel cell membranes under a range of controlled environmental conditions. A statistical

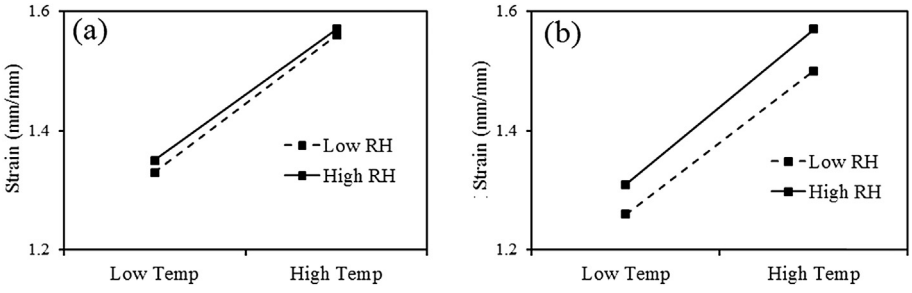

Fig. 10. Interaction plots for the strain at (a) $N_1 = 2 \times 10^5$ and (b) $N_4 = 8 \times 10^5$.

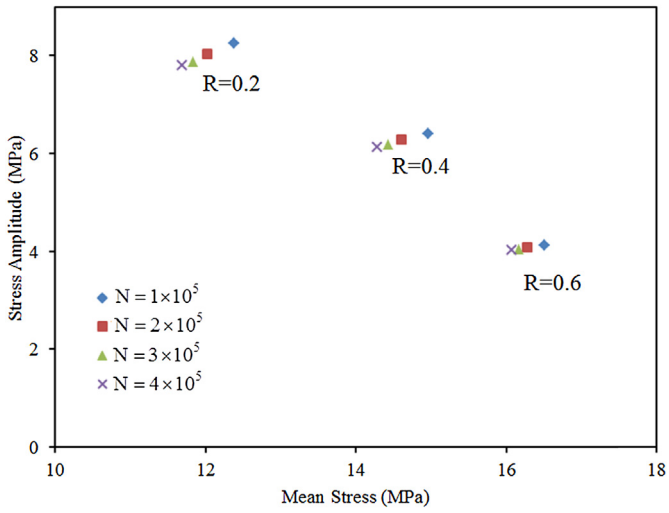

Fig. 12. Stress amplitude versus mean stress for three different stress ratios (R).

design of experiments approach was utilized to determine the effects of temperature and relative humidity on the maximum stress and final strain at rupture. The experimental results revealed that the membrane fatigue lifetime increases exponentially as the maximum stress is reduced. At a given stress level, the fatigue process was found to be much more severe at fuel cell conditions than at room conditions, and the lifetime was shown to decrease with increasing temperature and humidity. These trends are attributed to the lower tensile yield stress at hot and humid conditions, accompanied by increased plastic deformation. At a given fatigue lifetime, the same effect was observed by a downward shift in the S–N fatigue curves toward lower representative stress levels. The sensitivity of the lifetime to the stress level was also higher at fuel cell conditions. The ANOVA results confirmed the statistical significance of these findings and further demonstrated a counteracting (stiffening) interaction effect of temperature and humidity. Overall, the temperature was the dominant factor: high temperature led to rapid fatigue failures.

All membrane specimens elongated significantly during the fatigue process due to plastic deformation and creep. The strain at fracture was found to decrease exponentially with increasing fatigue lifetime. At a given fatigue life, a membrane exposed to fuel cell conditions was shown to accommodate more strain before fracture than one exposed to room conditions, as anticipated due to the softening of the material. Furthermore, normalization of the strain curves revealed that the total deformation of the membrane progressed in a specific manner regardless of the loading or ambient conditions, which indicates a consistent fatigue process supported by a consistent fracture based failure mode – as desired for a reliable fatigue test. The temperature was again the dominant factor: high temperature led to high strain. A critical level of strain dominated by plastic deformation was determined for fatigue fracture at fuel cell conditions.

The intended action of the fatigue test was verified by investigating different ratios of the minimum stress to maximum stress (R). As expected, the proposed R value of 0.2 led to fatigue dominated failures, while larger R values induced creep dominated ruptures due to the high mean stress.

In summary, the present ex-situ fatigue test is anticipated to be a viable method for rapid benchmarking of the mechanical stability of fuel cell membranes in the context of fatigue fractures caused by repetitive hygrothermal cycles during duty cycle operation. The findings of this work demonstrate the implications of increased level of cyclic mechanical stresses, temperature, and relative humidity on the membrane fatigue lifetime.

Acknowledgments

Funding for this research provided by the Automotive Partnership Canada (APC), Ballard Power Systems, and Simon Fraser University is highly appreciated.

References

[1] Y. Wang, K.S. Chen, J. Mishler, S.C. Cho, X.C. Adroher, Appl. Energy 88 (2011) 981.
[2] E. Kjeang, N. Djilali, D. Sinton, J. Power Sources 186 (2009) 353.
[3] W. Yoon, X. Huang, J. Electrochem. Soc. 157 (2010) B680.
[4] A. Nanjundappa, A.S. Alavijeh, M. El Hannach, D. Harvey, E. Kjeang, Electrochim. Acta 110 (2013) 349.
[5] J. Wu, X.Z. Yuan, J.J. Martin, H. Wang, J. Zhang, J. Shen, S. Wu, W. Merida, J. Power Sources 184 (2008) 104.
[6] U.H.N. Dürr, M. Gildenberg, A. Ramamoorthy, Chem. Rev. 112 (2012) 6054.
[7] H. Zhang, P.K. Shen, Chem. Rev. 112 (2012) 2780.
[8] S. Zhang, X.-Z. Yuan, R. Hiesgen, K.A. Friedrich, H. Wang, M. Schulze, A. Haug, H. Li, J. Power Sources 205 (2012) 290.
[9] N.L. Garland, T.G. Benjaminb, J.P. Kopaszb, ECS Trans. 11 (2007) 923.
[10] P. Trogadas, J. Parrondo, V. Ramani, Electrochem. Solid-State Lett. 11 (2008) B113.
[11] M. Lei, T.Z. Yang, W.J. Wang, K. Huang, Y.C. Zhang, R. Zhang, R.Z. Jiao, X.L. Fu, H.J. Yang, Y.G. Wang, W.H. Tang, J. Power Sources 230 (2013) 96.
[12] L. Gubler, W.H. Koppenol, J. Electrochem. Soc. 159 (2012) B211.
[13] L. Ghassemzadeh, T.J. Peckham, T. Weissbach, X. Luo, S. Holdcroft, J. Am. Chem. Soc. 135 (2013) 15923.
[14] N. Macauley, L. Ghassemzadeh, C. Lim, M. Watson, J. Kolodziej, M. Lauritzen, S. Holdcroft, E. Kjeang, ECS Electrochem. Lett. 2 (2013) F33.
[15] A.B. Laconti, M. Hamdan, R.C. Mcdonald, Handb. Fuel Cells Fundam. Technol. Appl. (2010) 1–16.
[16] C.S. Gittleman, F.D. Coms, Y.-H. Lai, in: M. Mench, E.C. Kumbur, T.N. Veziroglu (Eds.), Mod. Top. Polym. Electrolyte Fuel Cell Degrad, Elsevier, 2011, pp. 15–88.
[17] R. Borup, J. Meyers, B. Pivovar, Y.S. Kim, R. Mukundan, N. Garland, D. Myers, M. Wilson, F. Garzon, D. Wood, P. Zelenay, K. More, K. Stroh, T. Zawodzinski, J. Boncella, J.E. McGrath, M. Inaba, K. Miyatake, M. Hori, K. Ota, Z. Ogumi, S. Miyata, A. Nishikata, Z. Siroma, Y. Uchimoto, K. Yasuda, K.-I. Kimijima, N. Iwashita, Chem. Rev. 107 (2007) 3904.
[18] F.D. Coms, ECS Trans. 16 (2008) 235.
[19] M.A. Goulet, R.M.H. Khorasany, C. De Torres, M. Lauritzen, E. Kjeang, G.G. Wang, N. Rajapakse, J. Power Sources 234 (2013) 38.
[20] R. Solasi, Y. Zou, X. Huang, K. Reifsnider, Mech. Time-Depend. Mater. 12 (2008) 15.
[21] R. Solasi, X. Huang, K. Reifsnider, Mech. Mater. 42 (2010) 678.
[22] Y. Tang, A.M. Karlsson, M.H. Santare, M. Gilbert, S. Cleghorn, W.B. Johnson, Mater. Sci. Eng. A 425 (2006) 297.
[23] S. Kundu, L.C. Simon, M. Fowler, S. Grot, Polymer (Guildf) 46 (2005) 11707.
[24] P. Choi, N.H. Jalani, T.M. Thampan, R. Datta, J. Polym. Sci. Part B Polym. Phys. 44 (2006) 2183.
[25] Z. Lu, M. Lugo, M.H. Santare, A.M. Karlsson, F.C. Busby, P. Walsh, J. Power Sources 214 (2012) 130.
[26] M.B. Satterfield, J.A.Y.B. Benziger, J. Polym. Sci. Part B Polym. Phys. 47 (2009) 11.
[27] P.W. Majsztrik, A.B. Bocarsly, J.B. Benziger, Macromolecules 41 (2008) 9849.
[28] R.M.H. Khorasany, M.-A. Goulet, A.S. Alavijeh, E. Kjeang, G.G. Wang, R.K.N.D. Rajapakse, J. Power Sources 252 (2014) 176.
[29] X. Huang, R. Solasi, Y.U.E. Zou, M. Feshler, K. Reifsnider, D. Condit, S. Burlatsky, T. Madden, J. Polym. Sci. Part B Polym. Phys. 44 (2006) 2346.
[30] T.T. Aindow, J. O'Neill, J. Power Sources 196 (2011) 3851.
[31] M.F. Mathias, R. Makharia, H.A. Gasteiger, J.J. Conley, T.J. Fuller, C.J. Gittleman, S.S. Kocha, D.P. Miller, C.K. Mittelsteadt, T. Xie, S.G. Yan, P.T. Yu, Electrochem. Soc. Interface 14 (3) (2005) 24–35.
[32] Y.H. Lai, C.K. Mittelsteadt, C.S. Gittleman, D.A. Dillard, in: Proceeding of FUELCELL2005, 2005, pp. 161–167.
[33] S. Zhang, X. Yuan, H. Wang, W. Merida, H. Zhu, J. Shen, S. Wu, J. Zhang, Int. J. Hydrog. Energy 34 (2009) 388.
[34] A. Kusoglu, A.M. Karlsson, M.H. Santare, S. Cleghorn, W.B. Johnson, J. Power Sources 170 (2007) 345.
[35] C. Lim, L. Ghassemzadeh, F. Van Hove, M. Lauritzen, J. Kolodziej, G.G. Wang, S. Holdcroft, E. Kjeang, J. Power Sources 257 (2014) 102.
[36] A. Kusoglu, Y. Tang, M. Lugo, A.M. Karlsson, M.H. Santare, S. Cleghorn, W.B. Johnson, J. Power Sources 195 (2010) 483.
[37] Y. Tang, A. Kusoglu, A.M. Karlsson, M.H. Santare, S. Cleghorn, W.B. Johnson, J. Power Sources 175 (2008) 817.
[38] M.N. Silberstein, M.C. Boyce, J. Power Sources 195 (2010) 5692.
[39] M.N. Silberstein, P.V. Pillai, M.C. Boyce, Polymer (Guildf) 52 (2011) 529.

[40] H. Tang, S. Peikang, S.P. Jiang, F. Wang, M. Pan, J. Power Sources 170 (2007) 85.
[41] Y. Kai, J. Fuel Cell. Sci. Technol. 10 (2013) 021007.
[42] Y. Li, J.K. Quincy, S.W. Case, M.W. Ellis, D.a. Dillard, Y.-H. Lai, M.K. Budinski, C.S. Gittleman, J. Power Sources 185 (2008) 374.
[43] E. Moukheiber, C. Bas, L. Flandin, Int. J. Hydrog. Energy 39 (2014) 2717.
[44] Y.H. Lai, D.A. Dillard, in: W. Vielstich, H.A. Gaistager, H. Yokokawa (Eds.), Handb. Fuel Cells Adv. Electrocatal. Mater. Diagnostics Durability, vol. 5, John Wiley Sons, New York, 2009, pp. 403–419.
[45] T. Zarrin-Ghalami, A. Fatemi, Int. J. Fatigue 55 (2013) 92.
[46] Z. Lopez, A. Fatemi, Mater. Sci. Eng. A 556 (2012) 540.
[47] M.N. Silberstein, M.C. Boyce, J. Power Sources 196 (2011) 3452.
[48] R. Solasi, Y. Zou, X. Huang, K. Reifsnider, Mech. Time-Depend. Mater. 12 (2007) 15.
[49] N.S. Khattra, A.M. Karlsson, M.H. Santare, P. Walsh, F.C. Busby, J. Power Sources 214 (2012) 365.
[50] Z. Lu, C. Kim, A.M. Karlsson, J.C. Cross, M.H. Santare, J. Power Sources 196 (2011) 4646.
[51] M. Pestrak, Y. Li, S.W. Case, D.a. Dillard, M.W. Ellis, Y.-H. Lai, C.S. Gittleman, J. Fuel Cell. Sci. Technol. 7 (2010) 041009.